



Review of Models of RF Surface Resistance in High Gradient Niobium Cavities for Particle Accelerators Revision 1

P. Bauer

Fermilab, Technical Division

The following reviews the most important models of RF surface resistance and the Q -characteristic of superconducting resonators with particular emphasis of their specific impact on Q -slope. This review discusses several field dependent surface resistance contributions that can explain Q slope, such as thermal run-away, quenching of grain edges, interface tunnel exchange and grain-boundary resistance. This list, however, is not exhaustive. In some cases the surface resistance contribution is not quantified because precise measurements are lacking. The author also does not claim that this review is exhaustive. The attempt was made to apply the different surface resistance contributions to the case of a TESLA cavity in order to assess the importance and the particular signature of each effect on the Q characteristic of a TESLA cavity.

Many thanks to Anne-Marie Valente, Gigi Ciovati, Juergen Halbritter, Bernard Visentin, Claire Antoine, Sergio Calatroni, Alex Gurevich and Jens Knobloch for their suggestions, comments and more importantly their original work, which is summarized in part here.

Table of Contents

1) Introduction	3
2) BCS Surface Resistance	5
3) Beyond BCS (higher order corrections).....	12
4) Residual Resistance.....	14
5) Local Defect	16
6) Trapped Flux	17
7) Interface Tunnel Exchange	19
8) Grain Boundary Contribution	20
9) Field Enhancement on Grain Edges	22
10) Summary	26
References	28
APPENDIX A	30
APPENDIX B.....	32
APPENDIX C.....	35

1) Introduction

The surface impedance, Z_s , of any good conductor can be derived using the normal skin effect theory. An expression for the surface resistance, R_s , and the surface reactance, X_s , can be obtained by expanding the skin effect term given in (1) to first order in σ_1/σ_2 ^[1] in the case of a very good conductor ($\sigma_1 \ll \sigma_2$). σ_1 / σ_2 is the electrical conductivity related to the normal- / superconducting electrons. The local (complex) conductivity of a superconductor, σ_2 , can be derived from the BCS theory or the 2-fluid model.

$$Z_s = R_s + iX_s = \sqrt{\frac{i\omega\mu_0}{\sigma}} = \sqrt{\frac{i\omega\mu_0}{\sigma_1 - i\sigma_2}} \approx |\sigma_1 \ll \sigma_2| \approx \frac{1}{2}\omega^2\mu_0^2\lambda_L^3\sigma_1 + i\omega\mu_0\lambda_L \quad (\Omega) \quad (1)$$

To obtain the cavity quality factor, Q , from the surface resistance, R_s , the cavity geometry factor G given in equation (2) is needed (see Table 1 for the geometry factor of a TESLA single cell resonator). As will be discussed in this note, several resistance contributions need to be included in the calculation of R_s . Among them are the so-called BCS resistance, the residual resistance, as well as many others. The known contributions to the surface resistance are the subject of this review. The typical approach is to infer $R_{s,tot}$ from a measured Q with equation (2).

$$Q = \frac{G}{R_{s,tot}}, \quad G = \frac{\omega\mu_0 \int_V |\vec{H}|^2 dr^3}{\int_A |\vec{H}|^2 dr^2} \quad (\Omega) \quad (2)$$

The RF power deposited per unit surface can be calculated with (3), where H_{RF} is typically the peak-magnetic-field along the equator of the cavity. Other surface power terms, such as for instance resulting from field emission or dielectric loss have been omitted in (3). In a TESLA type cavity the ratio of peak magnetic field to average on-axis accelerating electric field is $B_{RF} = \mu_0 H_{RF} \sim 4 \text{ mT/MV/m}$.

$$P_s = \frac{1}{2} R_{s,tot} |\vec{H}_{RF}|^2 \quad \left(\frac{W}{m^2} \right) \quad (3)$$

Many of the R_s contributions depend on the strength of the fields on the cavity surface, either directly or indirectly. The most important

effect is resulting from the exponential temperature dependence of the so-called BCS surface resistance contribution (discussed in 2), which in turn leads to an increase of the equilibrium surface temperature with RF power and vice versa (via equ. 3). The models describing the increase of surface resistance with peak RF surface field are therefore commonly referred to as thermal feedback models.

The cavity Q is usually plotted as a function of average accelerating gradient, peak magnetic or peak electric field in the cavity. As shown in the example of **Figure 1** the typical Q vs B_{RF} curve is initially flat¹, determined solely by the residual resistance and (constant) BCS resistance. As the RF heat load rises with H_{RF}^2 , thermal feedback kicks in and Q starts to drop. This final precipitous drop of Q is usually referred to as Q -slope. Thermal runaway on the resonator surface due to thermal feedback, however, is a “natural” source of Q slope, and nothing can be done to reduce Q slope below it. It is expected to occur at fields close to the so-called RF critical field ($\sim B_{c,therm} \sim 180$ mT). The field level at which Q drop appears, however, can be much lower than the RF critical field, in which case additional surface resistance contributions are to be present. This note will illustrate the effect of

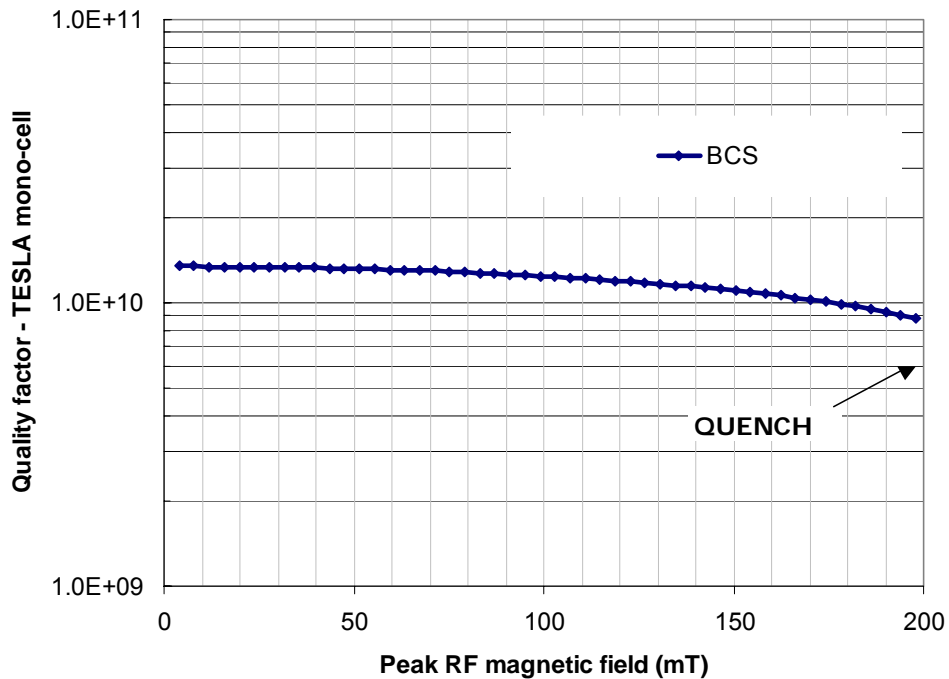


Figure 1: Calculated quality factor curve for TESLA single cell cavity (parameters in Table 1) with BCS surface resistance only (equ. 4c)

¹ In fact experimental Q curves are never entirely flat, even at low field, where a decrease of Q toward lower fields is often observed.

various known surface resistance contributions to the Q characteristic for the model case of a bulk Nb TESLA single-cell cavity.

An important part of the Q model is the iterative thermal model used to calculate the increase of surface temperature and surface resistance with increasing RF load. This model is discussed in detail in appendix A. The Nb heat conductivity was modeled using the parametrization proposed in Koechler and Bonin^[2] (see appendix B for further discussion). Their model includes the electron and phonon contributions to the thermal conductivity. Our model also includes the phonon peak, not included in the Koechler/Bonin model. The phonon peak dominates the thermal conductivity at 2 K. The thermal model also uses a phenomenological fit of the Kapitza impedance at the Nb-Hell interface. Using the thermal model to calculate the equilibrium surface temperature for a given amount of RF surface heating, the Q characteristic can then be computed from the surface resistance with equation (2). Table 1 summarizes the major parameters of TESLA superconducting cavities as assumed in the calculations presented here.

Table 1: Parameters of TESLA single cell cavity^[3].

Parameter	
Frequency (mode), f	1.3 GHz (TM010)
Bath temperature, T_0	2 K
Geometry factor, G	250 Ω
Residual magnetic field, B_{res}	< 1 μ T
Peak field to accelerating gradient factor, b_g	4 mT/MV/m
Cavity wall thickness (bulk Nb), d_w	3 mm
Grain size	50 μ m
RRR	> 300

2) BCS Surface Resistance

A theoretically rigorous derivation of the surface resistance of a superconductor on the basis of the BCS theory was implemented in a widely used program by Halbritter^[4]. The Halbritter program is based on the calculation of the scattering probability of RF photons at quasi-particles (=electrons thermally excited above the energy gap). The strength of the electron photon scattering is described with the matrix element $A(k)$, where k is the photon wave vector. $N(\varepsilon)$ is the density of states and $f(\varepsilon)$ is the Fermi-Dirac statistics function. For $T > 0$ the density of states above the energy gap, characteristic of

superconductors, is not zero. The integral is performed over the entire parameter space spanned by the initial, p_i and final electron momenta, p_f , as well as over all possible photon wave-vectors, k . C is a frequency dependent factor.

$$R_{s,BCS} \approx C(\hbar\omega) \left\{ \int_{-\Delta}^{\Delta} d\varepsilon 2[f(\varepsilon) - f(\varepsilon + \hbar\omega)] N(\varepsilon) N(\varepsilon + \hbar\omega) \int d^3k d^2p_i d^2p_f \right\} \left\{ \left| \langle p_i | A(k) | p_f \rangle \right|^2 \frac{1}{H_{II}^2} \right\} \quad (\Omega) \quad (4a)$$

Typical material parameters, such as the critical temperature, T_c , the London penetration depth, λ_L , the coherence length, ξ_{BCS} , and the energy gap parameter, $\Delta/k_B T_c$, used in the Halbritter-program are summarized in **Table 2**. Note that the Halbritter program uses a coherence length different from the BCS coherence length in **Table 2**. As a matter of different definition the “Halbritter coherence length” is related to the BCS coherence length with $\xi_{HR} = \pi/2 \times \xi_{BCS}$. Furthermore the implementation of the Halbritter program used here calculates the electron mean-free-path (*mfp*) from the *RRR*. To obtain the *mfp* stated in the table a “fake” *RRR* of 84 was used in the computations (otherwise the *RRR* was as stated in **Table 1**). Also note that the superconductor is usually polycrystalline with varying degree of purity from the surface into the bulk. Also some Nb-oxides (such as $NbO_{1\pm\delta}$) are normal-conducting or insulating and contribute to the surface resistivity. Typically these different contributions are not distinguished and therefore the material parameters in **Table 2** represent an average over the field-penetration depth. The energy gap parameter in the table, for example, is clearly smaller than expected in a Nb single crystal including strong coupling (1.85-1.92 with oxide - 2.05 without oxide –the “theoretical” material independent BCS value without strong coupling corrections is 1.76). Recent data^[5] obtained for state of the art Nb for RF cavities suggest slightly different material parameters than those listed in **Table 2**. For instance the coherence length ξ_{BCS} was found to be 29 nm, which would enhance the BCS surface resistance according to the Halbritter program by 15%.

A simplified formulation of the surface resistance of a superconductor can be obtained on the basis of the 2-fluid model^[6], which provides expressions for the AC conductivity σ_1 and the London depth $\lambda_L(\lambda_{L0}, \xi_{BCS}, l_{mfp})$ to calculate R_s with (1):

$$R_{s,BCS} \approx \frac{1}{2} \omega^2 \mu_0^2 \lambda_L^3 \sigma_1 = \frac{A}{2} \omega^2 \mu_0^2 \left(\lambda_{L0} \sqrt{1 + \frac{\xi_{BCS}}{l_{mfp}}} \right)^3 \frac{RRR}{\rho_n(300K)} e^{\left(\frac{\Delta(0)T_c}{k_B T} \right)} \quad (\Omega) \quad (4b)$$

with A being a material independent constant (best found from a comparison with measurement data). The two fluid model only gives qualitative guidance and is best for Nb in the “dirty” limit (low RRR, small mfp , $\kappa < 1$). It correctly shows, however, that the BCS surface resistance strongly rises with London depth, exponentially drops with the gap- energy, rises with coherence length and goes through a minimum for an optimum mfp as a result of the antagonistic effects of the mfp on the normal state conductivity ($\sigma_n = RRR/\rho_n(300K) \sim l_{mfp}$) and the London depth ($\lambda_L \sim 1/l_{mfp}$).

In practice, however, a phenomenological law of the type given in (4c) is most commonly used today [8]:

$$R_{s,BCS} \approx 1.643 \times 10^{-5} \frac{T_c}{T} (f(\text{GHz}))^2 e^{\left(\frac{1.92 T_c}{T} \right)} \quad (\Omega) \quad , \quad (4c)$$

where the constant factor 1.7 times larger than the similar expression in reference [8], the difference presumably being the result of recent improvements of the quality of SRF cavity surfaces. **Figure 2** compares the BCS surface resistance computed with the Halbritter BCS theory (4a) and the phenomenological fit (4c) for the specific case of the operational and cavity parameters discussed here (as listed in **Table 1** and **Table 2**).

Also note that the BCS surface resistance (4a) was calculated with the Halbritter program for the material parameters such as the mean free path or the energy gap, listed in Table 2. These parameters are often varied to fit the measured surface resistance. In this sense they are averages over the 50 nm surface layer that participate in the RF shielding. Their “direct” measurement, layer-by-layer, would further clarify the various contributions to the BCS resistance in “real” materials, such as the inter and intra-grain BCS contributions as well as the contribution of different layers with different degrees of purity and/or oxidation. It could also lead to the identification of other, yet unknown temperature dependent contributions to the surface resistance. Table 2 summarizes the Nb material parameters relevant for the calculation of the BCS contribution to the surface resistance (4a).

Table 2: Material parameters of superconducting Nb relevant for the calculation of the BCS surface resistance ^[6]. The coherence length in parentheses is that used as input into the Halbritter program. It is related to the BCS coherence length with $\xi_{HR}=\pi/2 \cdot \xi_{BCS}$.

critical temperature T_c (K)	coherence length ξ_{BCS} (nm)	London depth $\lambda_L(0)$ (nm)	gap energy $\Delta(0)/k_B T_c$	mean free path l_{mfp} (nm)	normal state DC resistivity (300K) ρ_n (Ωm)	normal state RF resistivity (10K, 1.3GHz, RRR300) $R_{s, norm}$ (Ω)
9.2	38(60)	40	1.86	500	14.5×10^{-8}	1.5×10^{-3}

Figure 2 shows the BCS surface resistance calculated with (4a) and (4b). The agreement between the two curves is reasonable.

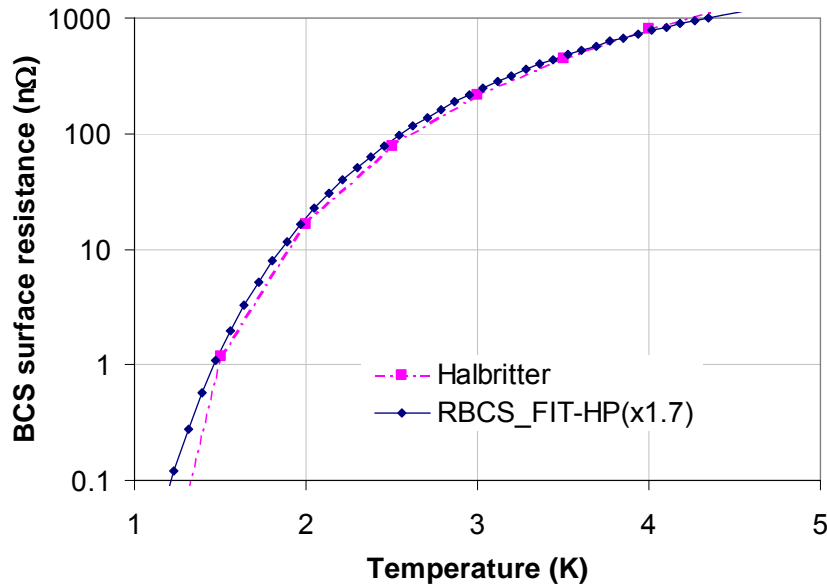


Figure 2: BCS surface resistance. Phenomenological fit (equ 4c) for TESLA type cavities (dashed) and as derived from BCS theory with the Halbritter program (equ. 4a) for “diffuse” reflection. Material parameters in Halbritter program as in Table 2.

Figure 3 shows the dependence of the BCS surface resistance on the mfp in the so-called “dirty” and “clean” limits. In a very clean superconductor with $l_{mfp} \gg \xi$, such as in today’s high purity Nb, the BCS resistance increases linearly with the mfp . As mentioned above the 2-fluid model indicates that this is related to the increase of normal state conductivity (increase of RRR) with purity and mfp (see equ. 4b). This, unfortunately is physically incorrect, since the normal state conductivity actually does not increase further with mfp in the clean limit because of the anomalous skin effect. The actual reasons

for this phenomenon are discussed in detail in [7]. As mentioned before the dirty limit is well described by the 2-fluid model. It even correctly predicts that the BCS resistance has its minimum for $l_{mfp} \sim \xi_0$.

“Engineering” of the mfp is a commonly pursued strategy to reduce the surface resistance in SCRF cavities. The example of the “mild bake”, a successful technological step to reduce Q-slope, is now believed^[9] to be one in which the mfp is changed in the thin RF active surface layer through oxide diffusion and the BCS resistance decreased from the clean limit. This, however, cannot explain completely the strong reduction of Q-slope after the low temperature bake^[24].

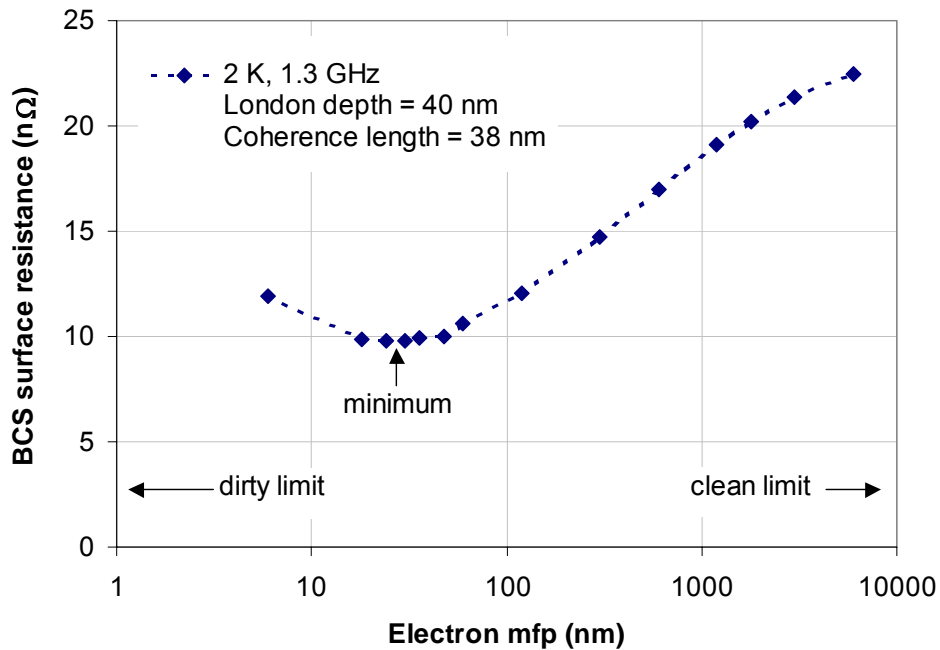


Figure 3: R_{BCS} and its dependence on the electron mfp calculated with the Halbritter model (for “diffuse” reflection). The dependence of R_{BCS} on the London depth is responsible for the fast increase for $mfp < 10$ nm, since the penetration depth increases with decreasing mfp. In the Halbritter model the increase of R_{BCS} at $mfp > 10$ nm is caused by photon momenta transferred between quasi-particle states having a kinetic energy difference matching optimally their density of states. The minimum occurs where $mfp \sim \xi_0$. A typical operating point in high purity Niobium is $mfp \sim 500$ nm. Material parameter used for Halbritter program as in Table 2. Note that the coherence length used in the Halbritter program is $\pi/2 \cdot \xi_{BCS}$, where ξ_{BCS} is the BCS coherence length assumed in this note.

Also the coherence length affects the performance of superconducting cavities, not only through its effect on the penetration depth. An increased coherence length also means more tolerance for “defects” such as normal inclusions and grain boundaries. Type I superconductors typically have large coherence lengths. There is, however, also the exponential dependence on the critical temperature

($R_{sBCS} \sim e^{-T_c}$), which favors type II and high T_c superconductors. “Clean-type II” superconductors, such as Nb, appear to offer the best compromise between high T_c and large ξ_0 .

Figure 4 shows a plot of the Q of a TESLA single cell cavity with the parameters as listed in **Table 1** with BCS surface resistance calculated with the material parameters in **Table 2**. The Q characteristic clearly shows the gradual increase of the BCS surface resistance with field as a result of thermal feedback. The thermal model and thermal conductivity used in the calculation are discussed in appendices A&B. Note that the thermal quench in this case is above the 200 mT field limit in the plot. SRF cavities to date have never performed at fields above ~ 180 m, which is believed to be close to the RF critical field. When the thermal parameters are reduced or the resistance increased the thermal quench field can become smaller than the critical RF field. Such a case will be discussed later in this review (for instance in section 9).

Often the heating effect on the surface resistance is taken into account using an analytical thermal feedback model ^[10]. Apart from the thermal conductivity, κ , (typically calculated at bath temperature, see appendix B), the thickness of the Nb sheet, d_w , the Kapitza conductance at the Nb-HeII interface, a_{Kap} , (see details in appendix B) the difficulty consists in the calculation of $\partial R_s / \partial T$. Assuming that $R_s = R_{sBCS}$, this term can be determined from equ. 4c.

$$\Delta T \propto \Delta P_{diss} \propto R_s H_s^2 / 2 \rightarrow R_s(T) = R_s(T_0) + \frac{\partial R_s}{\partial T} \Delta T \quad (5a)$$

$$R_s(T) = \frac{R_s(T_0)}{(1 - CE_{acc}^2)} \quad C \approx \underbrace{\frac{1}{2} \left(\frac{4 \cdot 10^{-9}}{\mu_0} \right)^2 \left(\frac{d_w}{\kappa_{Nb}} + \frac{1}{a_{Kap}} \right)}_{\sim 1.6 \cdot 10^{-9} (V/m)^2 \left(\frac{\Omega}{K} \right)} \frac{\partial R_s}{\partial T} \quad (5b)$$

Figure 4 also includes the Q -characteristic calculated for a TESLA single cell cavity (with BCS resistance only) with the analytical thermal feedback model. In the iterative surface temperature calculation model the temperature increase on the RF exposed surface is 150 mK at 200 mT surface magnetic field. At 100 mT surface field the temperature gradient across the 3 mm thick Nb sheet is 17 mK. The temperature step at the Nb-HeII interface is 11 mK. The BCS surface resistance

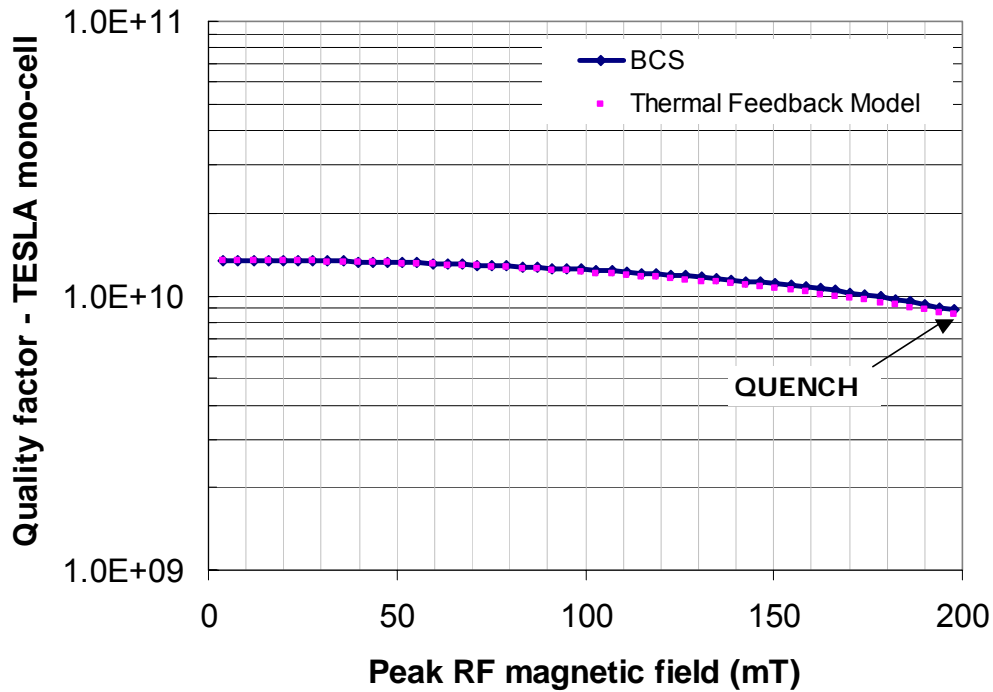


Figure 4: Quality factor curve for TESLA cavity (parameters in Table 1) with BCS surface resistance only (equ. 4c). For comparative purposes the calculations using the analytical thermal feedback model are also shown (equ. 5a-b).

changes from 19 nΩ at zero field (where only the Kapitza interface conductance contributes to the ΔT on the RF surface) to 29 nΩ at 200 mT peak surface field. The analytical model was made to agree with the numerical model using $\partial R_s / \partial T \sim 0.1 \text{ n}\Omega / \text{mK}$ (calculated at $T_0 + 100$ mK with (4c)) and $R_s(T_0) = 18.6 \text{ n}\Omega$ (obtained from (4c)) and consistent with fits of data, [24].

Although the analytical thermal feedback model describes the Q-drop very well in the above case, the more accurate iterative model was used in the subsequent calculations. This, because the thermal feedback model is only applicable at fields much lower than the thermal breakdown field (= field at which thermal runaway occurs). This is the case here, where the thermal breakdown field is much larger than the RF critical field (and beyond the range of field shown).

Increase of surface resistance and quench close and at the RF critical field is not included in the model above. These effects will be discussed next.

3) Beyond BCS (higher order corrections)

Several corrections and additions to the BCS resistance effect have been mentioned as possible causes for Q-slope or deviations from the BCS behavior at high fields. Many of them still lack “clear-cut” experimental evidence. Some of them are listed in the following.

It is well known that the superconducting gap parameter is suppressed in the presence of metallic oxides or foreign phases. An issue, which is mentioned in chapter 2, is that the superconducting gap parameter used to fit experimental results with Halbritter’s BCS program is rather a fit-parameter than the result of an in situ measurement. Gap profiles across the “active” layer of state of the art material would tell us if the values we typically use to fit cavity test results are indeed averages over the RF field penetration layer. **Figure 5** shows the effect of the gap parameter on the surface resistance as calculated with the Halbritter model. It is clear that the effect is not negligible and that larger gap parameters, such as found in clean single crystals, result in less $R_{s,BCS}$.

An especially interesting issue is that of RF field amplitude dependent corrections to the BCS surface resistance. It is known that at temperatures close to T_c the gap energy becomes strongly dependent on the amplitude of the super-current and thus on the amplitude of

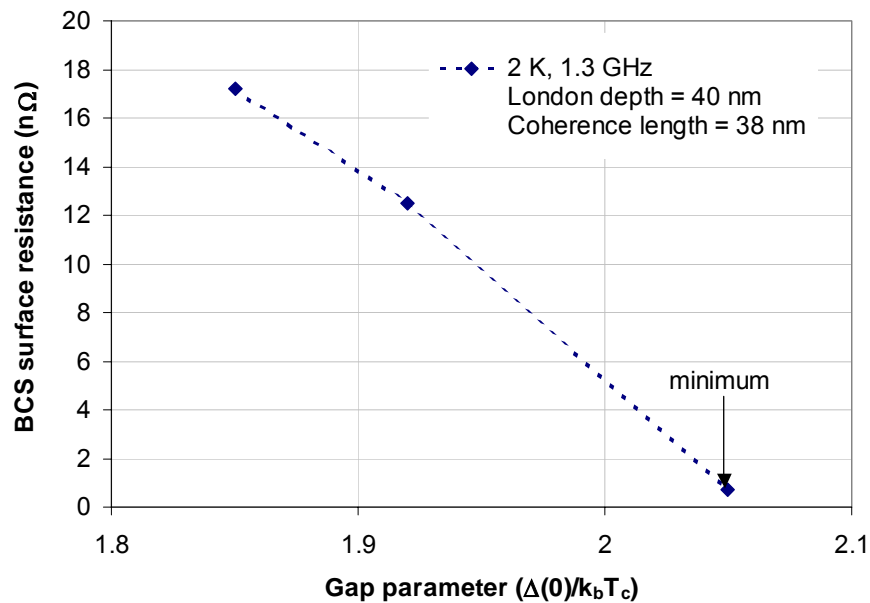


Figure 5: R_{BCS} and its dependence on the gap parameter calculated with the Halbritter model (for “diffuse” reflection). Material parameter used for Halbritter program as in Table 2.

the RF field. Equ. (6) gives a first order expansion of the non-linear BCS contribution. Higher order terms also exist. The parameter α depends on frequency and increases at reduced temperature. The RF critical field is not known well today. In an ideal sample in the DC condition flux vortices enter the material at the thermo-dynamic critical field $H_{c,therm}$. Therefore the critical field is believed to be in some way related to this field.

$$\mathbf{R}_{s,BCS}(\mathbf{B}) \approx \mathbf{R}_{s,BCS}(\mathbf{B} \sim 0) \left(1 + \alpha \left(\frac{\mathbf{B}_{peak}}{\mathbf{B}_{c,crit}} \right)^2 \right) \quad (\Omega) \quad (6)$$

A smaller, but similar effect could be the result of the temperature dependence of the gap parameter as mentioned by Valente ^[14]. The effect, as described by equ. (7), however, appears to be very small at the temperatures at which SRF cavities are typically used (~2 K). Also, the Halbritter model discussed in section 2) includes this effect.

$$\Delta(T) = \Delta(0) \sqrt{\cos \left[\frac{\pi}{2} \left(\frac{T}{T_c} \right)^2 \right]} \quad (7)$$

4) Residual Resistance

The residual surface resistance is typically assumed to be the saturation value to which the surface resistance tends at very low temperatures ($T < 1.5$ K), when the BCS resistance becomes negligible. This is illustrated in **Figure 6**, which shows the surface resistance versus temperature. Little is known about the origins of the residual surface resistance. It is known to increase with frequency. It is believed to be related in part to the surface oxides. The oxide layer on the Nb typically consists of less than 0.5 nm of NbO_x ($x \leq 1$) and 1-3 nm of $\text{Nb}_2\text{O}_{5-y}$, covered with hydrogen bonded $\text{H}_2\text{O}/\text{C}_x\text{H}_y(\text{OH})_z$ of similar thickness^[11]. Typically surface resistances in the range 1-20 n Ω are found in TESLA cavities (1-10 n Ω in Cern sputtered cavities).

One possible source of residual resistance is dielectric loss. Equ. 8 gives the surface resistance contribution, as calculated from the dielectric layer thickness, d_e , the loss tangent, $tn\delta_e$, and the permeability, ϵ_R . This formula can easily be applied to the case of

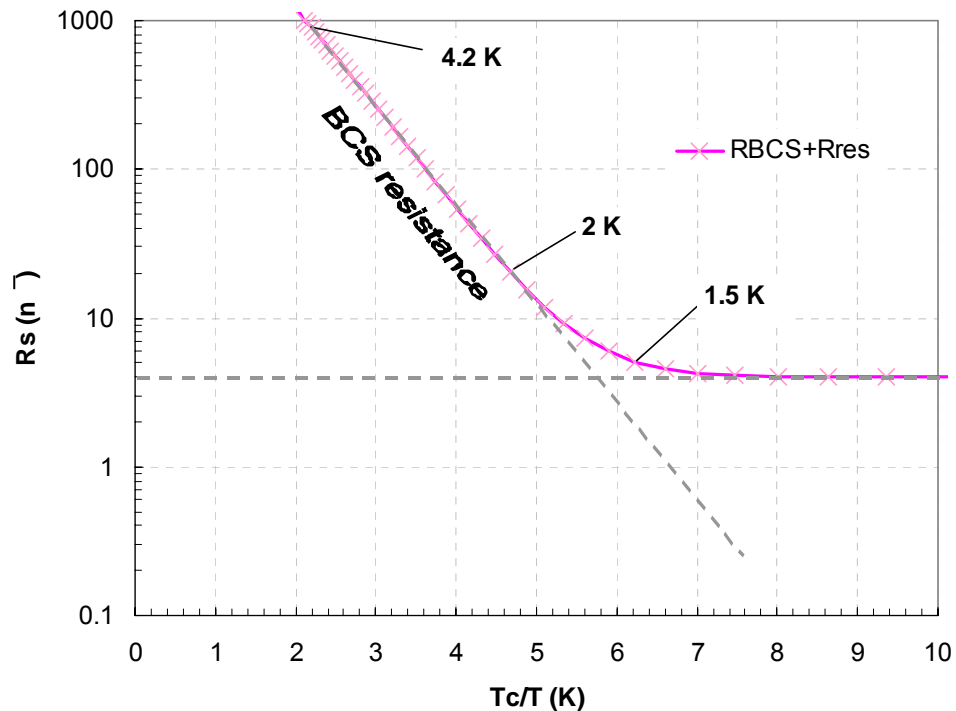


Figure 6: Surface resistance in Nb (BCS resistance as calculated with equ. (4c) and 4 n Ω residual resistance) as function of inverse temperature (T_c is the critical temperature – see Table 2). This plot clearly shows how the measurement of surface resistance at several temperatures allows separation of the temperature dependent resistance contributions, such as the BCS resistance, from temperature independent contributions, such as the residual resistance.

magnetic RF losses substituting the loss tangent and permeability with their magnetic equivalents. For $d_e \sim 5$ nm, $tn\delta_e < 10^{-5}$ and $\epsilon_r \sim 10$ equation (8), however, gives less than 0.1 nΩ for a TESLA cavity. **Figure 7** shows the Q of a TESLA cavity with BCS resistance and different amounts of residual resistance, varying from zero to 20 nΩ. Over almost the entire field range the residual surface resistance causes an almost constant Q reduction.

$$R_{s,DE} = \omega\mu_0 d_e \frac{tg\delta_e}{2\epsilon_r} \quad (\Omega) \quad (8)$$

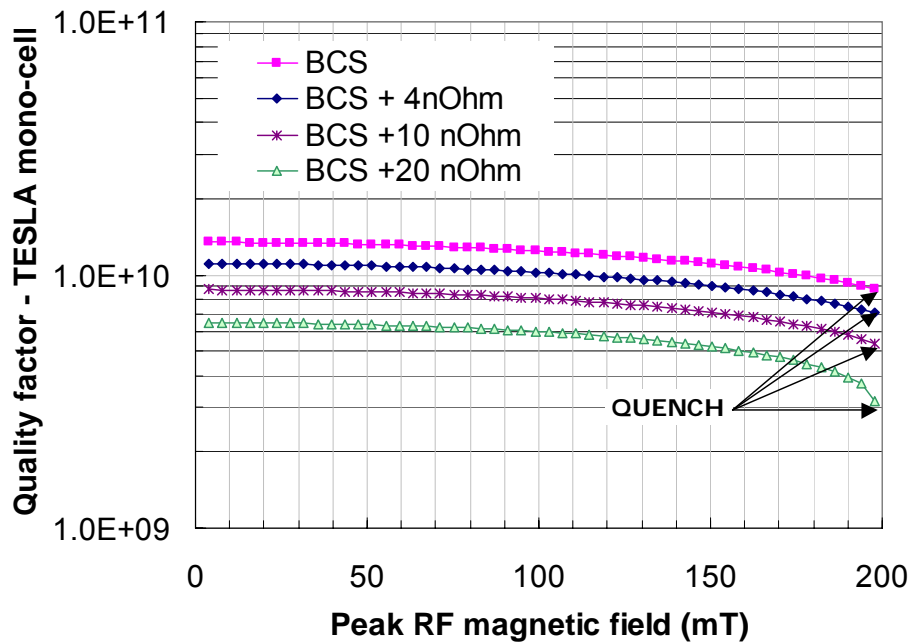


Figure 7: Quality factor curve for TESLA cavity (parameters in Table 1) with BCS surface resistance (equ. 4c) and 4, 10 and 20 nΩ residual resistance.

Note that the lowest surface resistance found thus far in bulk Nb cavities was 0.5 nΩ ($Q \sim 2 \times 10^{11}$) at up to medium fields at 1.6 K in Saclay cavity C117 [16]. Such a low R_s , however, is usually not sustainable at high gradients.

5) Local Defect

A simple model proposed by C. Lyneis (and well described in Padamsee^[8]) assumes that the defect of characteristic size d (e.g. a normal conducting inclusions) is thermally isolated from the surroundings and directly cooled by the superfluid helium. In this case the temperature of the defect can be derived from the equivalence of the RF power generated in the defect and the RF power conducted through the defect to the helium at bath temperature T_0 (the thermal conductivity of the defect being κ). As a further simplification, the Kapitza resistance at the Nb/He interface is neglected. It is assumed that the cavity quenches when the temperature in the defect reaches the critical temperature. This condition provides an expression for H_{max} , the surface field at which the quench occurs. According to this very simple model the surface resistance due to a defect can be described with:

$$R_{s,def} = \begin{cases} \sim 0 & H < H_{max} \\ R_{s,norm} & H \geq H_{max} \end{cases} \quad (\Omega) \quad H_{max}(d) \approx \sqrt{\frac{4\kappa(T_c - T_0)}{dR_{s,norm}}} \left(\frac{A}{m} \right) \quad (9)$$

Figure 8 shows the quality factor as a function of peak field in a TESLA cavity with and without defect. The signature of the defect according to this model is essentially a pre-mature quench.

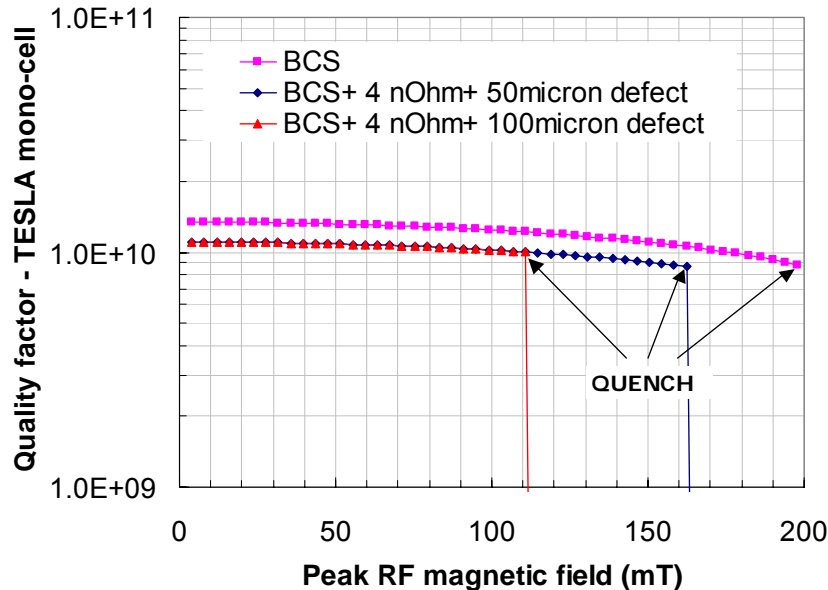


Figure 8: Quality factor curve for TESLA cavity (parameters in Table 1) with BCS surface resistance only (equ. 4c) and with BCS resistance, residual resistance (4 nΩ) and a 50 μm as well as a 100 μm normal conducting defect, causing premature quenches. The discrepancy between the Q curves before the quench is the result of the residual resistance.

6) Trapped Flux

The simplest model ([8], p.174) describing the effect of trapped flux on the RF surface resistance is based on the assumption that all external field is trapped in the superconductor. An estimate of the total resistive area represented by the normal conducting core-regions of trapped flux vortices, each of surface $\sim \pi \xi_0^2$ is obtained from the number of flux-quanta contained in the given residual field, B_{res} , by division through the flux quantum ϕ_0 . Using a standard definition of H_{c2} (the field at which all surface is covered by fluxons) and the normal state surface resistance $R_{s,norm}$ (~ 1.5 m Ω at 1.3 GHz) one obtains the following surface resistance contribution:

$$R_{s,mag} = \frac{B_{ext}}{2B_{c2}} R_{s,norm} \quad (\Omega) \quad (10)$$

According to this simple model, the surface resistance contribution of trapped flux is a constant and independent of the RF field amplitude (as well as the angle between the external field and the RF field). It would therefore affect the Q-characteristic of a cavity in the same way as a residual resistance. **Figure 9** shows the effect of trapped field on the surface resistance as calculated with equ. (10).

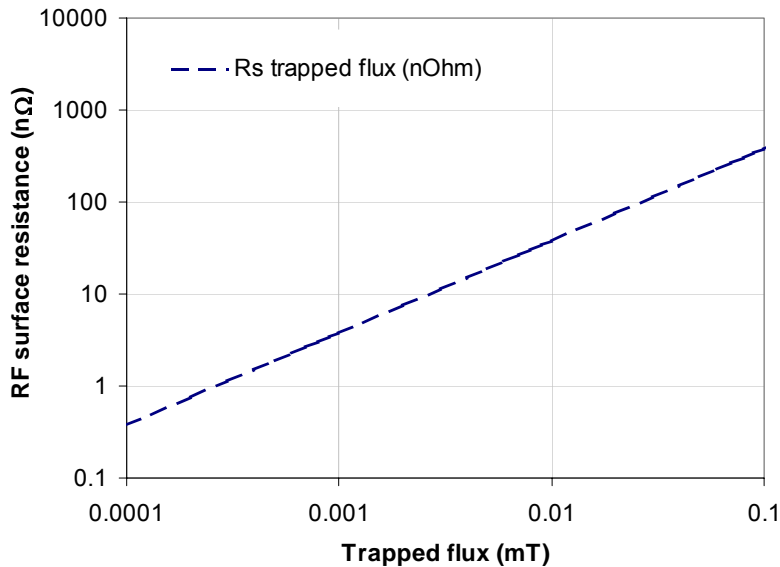


Figure 9: RF surface resistance in Nb as function of trapped flux calculated with the simplest possible model, which assumes that all flux is trapped in the superconductor. The simple model also neglects flux-flow in the RF field. The TESLA accelerator design includes magnetic shielding down to 0.001 mT.

This simple model predicts the external field effect reasonably well. This, however, appears to be a fortuitous coincidence if one considers that in the case of sputtered Nb films, the magnetic field dependence is hundred times weaker, a fact that the above model cannot explain^[14]. Extensive measurements on sputtered Nb films indicate not only a hundred times smaller surface resistance at the same trapped flux at low fields than predicted with equ. 6, but also field (weak, $R_{s,mag} \sim H_{RF} H_{ext}$ at low RF field amplitudes) and temperature effects (~two-fold increase between 2-4 K).

Although mere speculation at this point, a possible explanation for the reduced surface resistance for a given external flux could be strong pinning in the sputtered film. The reason for the H_{RF} and temperature dependence of $R_{s,mag}$ in sputtered films could then be flux-line depinning at larger Lorentz-forces or temperature activation. Existing flux-movement-models need to be revisited if indeed the trapped field effects turn out to be related to flux motion in the RF field. The presence of magnetic flux in the films is generally not unexpected. One of the models to explain the increased Q slope in sputtered Nb cavities assumes the presence of so-called Josephson flux-lines in the grain-boundaries and associated hysteresis losses in the RF fields.

7) Interface Tunnel Exchange

Oxides in the surface dielectric provide localized states accessible to sub-gap electrons in the adjacent superconductor via tunneling. Once occupied resonant absorption of RF fields and scattering on phonons generate the loss contribution^[11]. This phenomenon is known from Josephson junctions. A derivation of the ITE related surface resistance contribution would certainly exceed the purpose of this review. Instead we present a phenomenological law proposed by J. Halbritter describing the effect of ITE on the RF surface resistance. This fit is given in equ. (11), where C is ~ 20 MV/m, b_g as given in **Table 1** and B_{peak} , the peak magnetic field in mT. This exponential surface resistance was implemented in the Q-calculation model for two possible values of l_{ITE} . The results are shown in **Figure 10**. Note that the cases with ITE resistance contributions end in a thermal quench below 200 mT, while the cases without are assumed to quench as a result of the critical field (assumed to be 200 mT) rather than thermal runaway.

$$R_{s,mag} = 2\pi f \mu_0 I_{ITE} e^{-\frac{Cb_g}{2B_{peak}(mT)}} \quad (\Omega) \quad (11)$$

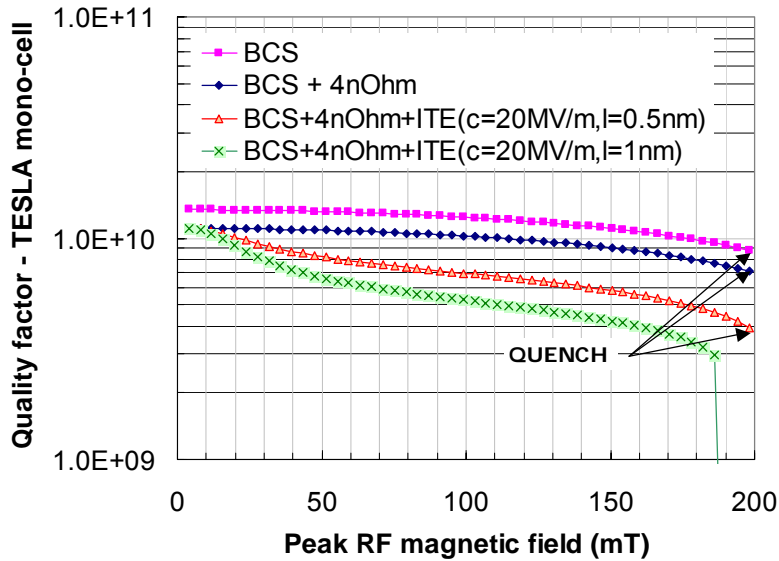


Figure 10: Quality factor curve for TESLA cavity (parameters in Table 1) with BCS surface resistance only (equ. 4c), with BCS resistance and residual resistance (4 nΩ) and two possible ITE scenarios with l_{ITE} 0.5 nm and 1 nm.

8) Grain Boundary Contribution

Initially the Q-slope in sputtered cavities was attributed to hydrides. Sputtered cavities cannot be heat-treated at high temperatures such as is commonly done in bulk cavities to outgas the hydrogen. This hypothesis was shown to be wrong^[19]. The strong Q-slope observed in sputtered Nb on Cu cavities is now believed to be in part the result of its much smaller (μm) grain-size as compared to the 100 μm grains in bulk Nb cavities and possibly the result of vortex penetration. Experiments with sputtered cavities with films of varying grain-size between 0.1–10 μm using different sputtering substrates indicated that the larger grain-size material had larger residual surface resistance. This appears counter-intuitive, but could be explained (according to Halbritter) by the fact that the amount of impurities in the pre-cursor material is constant and therefore the grain-boundary contamination is more pronounced the less grain boundary there is (and the larger the grains). The effect of impurity segregation at the grain boundaries (GB) on the surface resistance was demonstrated^[18].

The effect of grain-boundaries on the RF surface resistance, however, is not well known. Models used for the description of high-Tc superconductors in which the grain-boundaries are described as weak links, were adapted to the case of RF fields. An example is the surface resistance formula from [17], given in equ. (12), which calculates the surface resistance in a weak-link lattice with lattice parameter a . The most important input parameter in this case is the grain boundary critical current density, $j_{c,GB}$.

$$R_{s,GB-WL} = \frac{\mu_0 \hbar (2\pi f)^2}{4\Delta(0)} \frac{\hbar / (2\mu_0 e a j_{c,GB})}{\sqrt{\lambda_L^2 + \hbar / (2\mu_0 e a j_{c,GB})}} \quad (\Omega) \quad (12)$$

Figure 11 shows the result of a calculation of the surface resistance as a function of the grain-boundary critical current density with equ. (12) for a weak link lattice parameter $a \sim 50 \mu\text{m}$ (grain size of typical high purity Niobium used for cavities). The de-pairing current density derived from the Meissner shielding condition, $j_{dp} \sim H_{c,therm} / \lambda_L(0)$, gives $\sim 3 \text{ MA/mm}^2$. At that current density the surface resistance contribution due to (12) would obviously be negligible. Nobody knows how to measure the grain-boundary de-pairing current density. Note that pinning critical current density measurements typically give results of the order of $j_c \sim 10^4 \text{ A/mm}^2$ in state of the art material^[5]. The fact that today's SRF cavities made from polycrystalline material achieve surface resistances of 10 n Ω and less indicates that grain

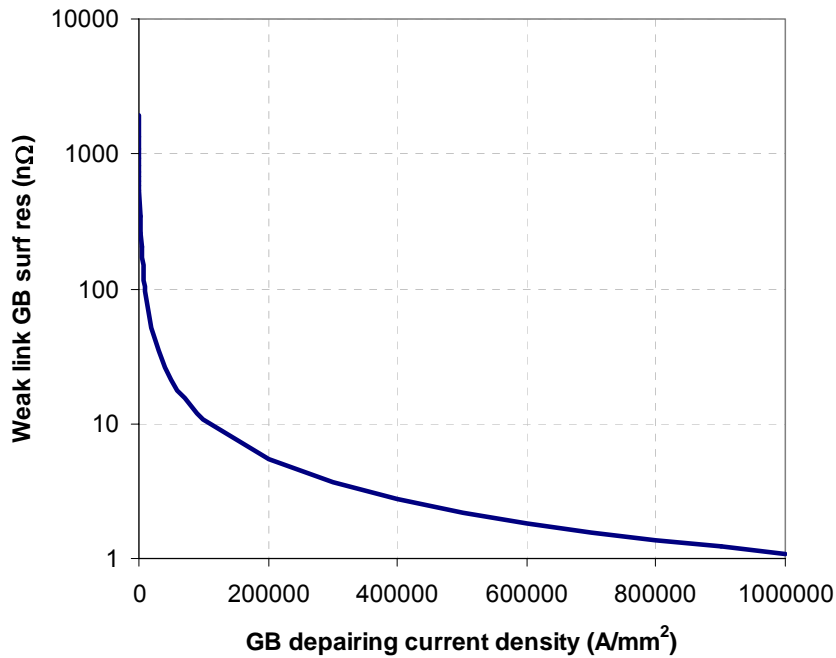


Figure 11: Surface resistance contribution in weak link model.

boundary effects can only be the cause of surface resistance contributions that are of the order of 1-10 nΩ. Probably more relevant than the weak-link effects (note that the coherence length in Nb is 2 orders of magnitude larger than in high temperature superconductors where weak link effects matter) are other aspects of the grain boundaries, such as for instance preferential flux-vortex penetration due to a reduced (or suppressed) gap parameter in the presence of oxides or metallic phases.

Also, grain-boundaries affect bulk and sputtered Nb cavities differently. For instance the elastic electron mean free path (~500 nm) is much shorter than the grain size in polycrystalline bulk niobium cavities today, but longer than the grain in the sputtered case. Therefore thermal conductivity, RRR and other transport properties vary with grain size in the case of sputtered cavities, but not in bulk cavities. Measurements of the normal state resistivity of the grain boundaries presented in [25] indicate that the grain boundaries dominate the resistivity (at least in the normal state). The specific grain boundary resistance was found to be $2 \cdot 10^{-13} \Omega \text{m}^2$, which for a 1 mm^2 junction between 2 grains becomes 100 nΩ. It is not clear what the implications of this result for the superconducting state are (when the grain boundaries become superconducting by proximity effect).

9) Field Enhancement on Grain Edges

Q slope can be explained by any surface resistance contribution with strong field dependence. One such contribution, proposed by J. Knobloch^[12], is given by field enhancement at the sharp edges of grains. This contribution is characterized by a strong dependence on field above a given threshold. Especially BCP etched surfaces are usually rougher with sharp grain-edges, believed to be the result of preferential etching at the grain boundaries. FE computations with electro-magnetic field codes reveal that field enhancement factors of up to two occur at the sharp edges of grains. Localized quenching of grain edges occur whenever the enhanced fields reach the critical field. This of course occurs preferably in the peak field (equator) regions.

Knobloch's model is based on an estimation of the total cavity surface quenched at a given field level in the cavity. To estimate the number of quenched grain edges, the model requires as an input the number of grains in the peak-field region and an enhancement factor distribution function. The number of concerned grains, $N_{gb,tot}$, can be calculated approximately from the effective area, A_{eff} , and the grain size, l_{gb} , (14). The effective area is the theoretical surface the cavity would have if the magnetic field everywhere on the surface would be at the peak field, H_{peak} , (13). It can be computed with any electromagnetic code capable of simulating the surface field distribution in the cavity. U is the cavity stored-energy, G is the geometry factor defined in (2).

$$A_{eff} = \frac{\oint H^2(x) d^2x}{H_{peak}^2} = \frac{2\omega U}{GH_{peak}^2} \quad (m^2) \quad (13)$$

$$N_{gb,tot} = \frac{A_{eff}}{l_{gb}^2} \quad (14)$$

The normalized distribution (N is the normalization factor) of enhancement factors, β , is Gaussian, (15), with mean and width derived from the following plausibility arguments. The field enhancement factor β at which this distribution peaks, β_0 , for example, is approximately the field at which the Q-slope starts (e.g. $H_{crit}/H_{slopestart} \sim 1.6$). The width of the distribution is bounded by the fact that enhancement factors above two are not consistent with typical surface roughness. The distribution parameters can be optimized by comparison of the model results with the experimentally observed Q-

slope. This procedure, however, assumes that the experimental Q-slope is caused mostly by field enhancement at the grain edges. The distribution function, (12), proposed by Knobloch uses $\beta_0 \sim 1.44$ and $\sigma \sim 0.0068$.

$$n(\beta) = \frac{1}{N} e^{-\sqrt{|\beta-\beta_0|}/\sigma} \quad \beta = \frac{H_{crit}}{H_{peak}} \quad (15)$$

The number of quenched grain boundaries can then be calculated from the total number of grain boundaries, $N_{gb,tot}$, and the convolution of the field enhancement factor distribution over all fields between H and H_{peak} .

$$N_{gb,qu}(H_{peak}) = N_{gb,tot} \int_{\beta(H_{peak})}^{\infty} n(\beta) d\beta \quad (16)$$

(17) gives the surface resistance contribution due to quenched grains as a function of the normal state surface resistance, the “width” of the quenched grain edge, w_{nc} , and $R_{s,norm}$ the surface resistance of Nb in the normal state ($\sim 1.5 \text{ m}\Omega$ at 1.3 GHz – see appendix C). **Figure 12** shows the result of a calculation of the field enhancement effect for $\beta_0 = 1.0-1.2$ and $\sigma = 0.001 - 0.01$ (grain size $50 \text{ }\mu\text{m}$, RF critical field $B_{crit} = 200 \text{ mT}$). Note that as the average field enhancement factor in (17) β_0 was used. The example in **Figure 12** shows that the surface resistance contribution of the quenched grain edges rises sharply ($\propto B_{peak}^4$) above the threshold set by B_{crit}/β_0 . The calculation indicates that $\sim 0.1\%$ of the grain edges have to be quenched for this effect to contribute significantly to the Q slope at $\sim 25 \text{ MV/m}$ accelerating gradients (100 mT peak field) in TESLA cavities. When all grain edges are quenched the surface resistance saturates. The saturation value is given by the normal surface resistance times the surface ratio of the sum of the grain boundaries and the effective cavity surface ($R_{s,norm} \times N_{gb,tot} \times l_{gb} \times w_{nc} / A_{eff}$).

$$R_{s,GB}(H_{peak}) = R_{s,norm} \beta_0^2 \frac{l_{gb} w_{nc} N_{gb,qu}(H_{peak})}{A_{eff}} \quad (\Omega) \quad (17)$$

The temperature rise in the superconducting regions adjacent to the quenched grain leads to a modest increase of the power generation (15%), which has not been factored into the calculations presented here. Knobloch’s thermal FE calculations indicate that such quenched

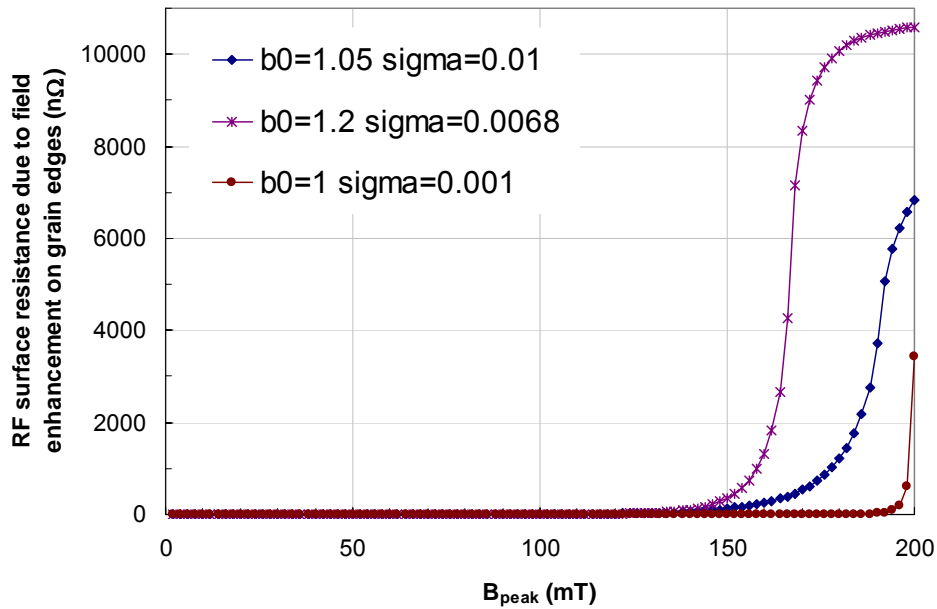


Figure 12: Surface resistance contribution in TESLA cavity due to field enhancement on grain boundary edges calculated with Knobloch model (model parameters: β_0 and σ are the mean and half-width of the Gaussian field enhancement factor distribution at the grain corners). The critical field was assumed to be 200 mT.

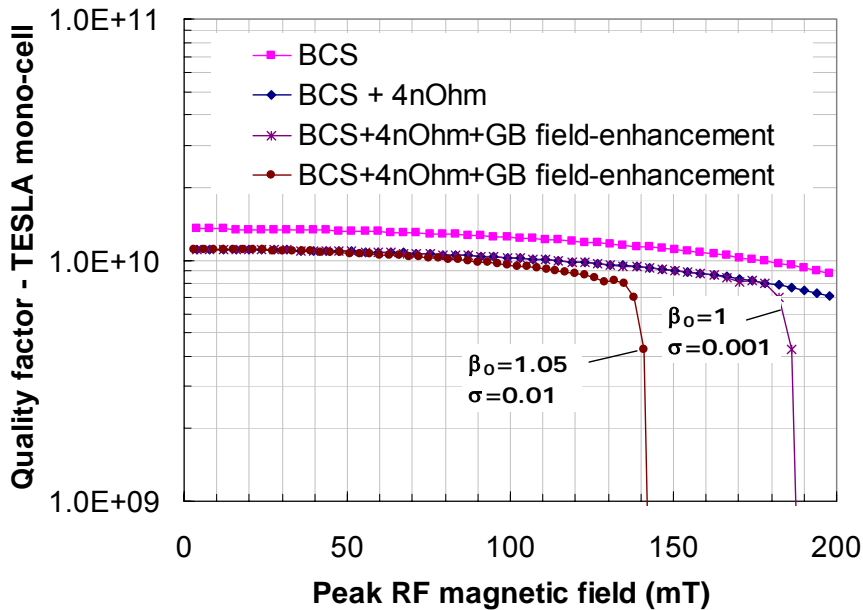


Figure 13: Quality factor of a TESLA single cell cavity with BCS resistance, residual resistance and grain edge quenching according to the Knobloch-model. The parameters of the grain edge quenching model are: 50 μm grain size, field enhancement factor distribution: $\beta_0=1\&1.05$, $\sigma=0.001\&0.01$, critical field 200 mT. See Figure 12 for the functional shape of the surface resistance contribution due to field enhancement on grain boundary edges calculated with the Knobloch model.

grain edges can be sustained up to very high fields before thermal runaway, leading to cavity quenches, occurs.

There is no doubt that the quenching of grain edges is a real effect. The grain-edge field enhancement model can even explain the smaller Q slope after the mild bake through the increase of the critical RF field through an increase in H_c (although the relationship between the critical RF field and the thermodynamic critical field is heavily discussed, there is no evidence contradicting the existence of a connection). It cannot, however, explain why some cavities with rough surfaces have operated with very little Q slope (CEA one-cell prototypes C1-15 and C1-16 ^[13]). It also can't explain why in some cases electropolished and BCP-etched cavities show the same Q slope before the mild bake (see for instance a discussion of such an example in [13]). Most likely the field enhancement is always there, but it is only one among several contributions to the observed Q slope and the above model probably overestimates its impact.

10) Summary

This review discussed in more or less detail the major known RF surface resistance contributions in high gradient bulk niobium cavities. Among them are the BCS resistance, the residual resistance, local defects, trapped flux, interface tunnel exchange and the effects related to grain boundaries and edges. It appears that the least known contributions are those related to the complexities of the real surface conditions in the cavities (as opposed to idealized surfaces). A one-dimensional model of the RF surface that assumes that on one side of the interface is single crystal Niobium and on the other RF fields in vacuum is certainly not consistent with the complex variety seen in the experiments. **Figure 14** shows a sketch of the known components of the “real” RF surface as suggested by J. Halbritter. The material-science in support of the superconducting RF cavity technology, I believe, still has long ways to go before the many possible implications of the complex surface topology, chemistry,..etc, on the RF behavior are fully understood.

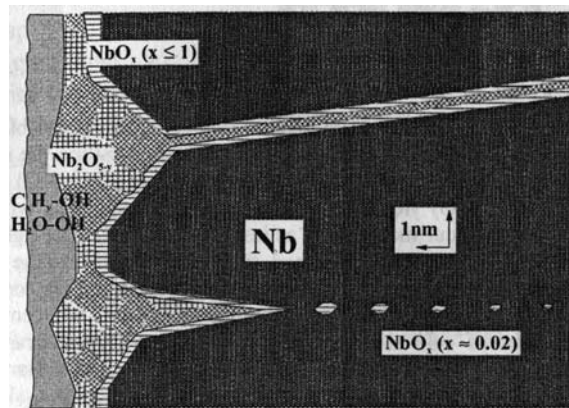


Figure 14: Nb surface with crack corrosion by oxidation by Nb_2O_5 volume expansion. Nb_2O_{5-y} weak links extend up to several RF penetration depths.

Some of these implications are:

- It is well known, for instance, that the Nb is coated by ~1-3 nm of oxide. Some of the NbO_x phases are metallic (or even superconducting) and contribute to the surface resistance. These contributions need to be understood (see the chapters on interface tunneling exchange, residual resistance, BCS resistance).
- The “real” material is poly-crystalline and grain boundaries are believed to play an important role, either through weakened superconductivity (“weak-link”) or through their interactions with

external magnetic flux. There are phenomena such as “crack-corrosion” that produce deep cracks in the Nb further exacerbating the problem. Also the weakening of the superconducting state on the grain surface as a result of the presence of oxides and defects is expected to play an important role.

- The grain-boundaries also play a role as areas where defects and contaminants gather. It is well known that contaminants affect for instance the BCS surface resistance and the thermal conductivity.

At the same time it is important to stress that the last 10 years have brought spectacular advances in the field of bulk Nb resonators, indicating that the material is now better understood than ever. Among these achievements are:

1. better thermal stability and reduced number of normal conducting defects due to higher purity Nb,
2. reduction of field emission as a result of high pressure water rinsing,
3. the mitigation of Q-disease via H out-gassing,
4. the increase of quench fields related to electro-polishing (reduction of sharpness of grain edges?) and to the mild in situ bake, that strongly mitigates Q slope possibly as a result of weak contamination (“doping”) with oxygen;

Several effects still lack good models and experimental data to be quantified. Among them are the effects of grain boundaries and the effects of variations of the parameters characterizing the superconducting state from the surface into the bulk. Also, little experimental research has been directed toward the elucidation of the interface tunnel exchange effects. References [21 – 24] give an up-to-date account of the surface resistance issues under discussion today.

References

- [1] A. Porch, "High Frequency Electromagnetic Properties", pp.99 in "Handbook of Superconducting Materials", Institute of Physics, D.A. Cardwell, D.S. Ginley – editors;
- [2] F. Koechlin, B. Bonin, "Parametrisation of the Niobium Thermal Conductivity in the Superconducting State", CEA internal note DAPNIA-SEA-96-01, Jan. 1996;
- [3] TESLA TDR, R. Brinkmann et al. editors, DESY, March 2001
- [4] J. Halbritter, "Fortran Program for the Computation of the Surface Impedance of Superconductors", Internal Note KFZ Karlsruhe 3/70-6. June 1970;
- [5] S. Casalbuoni et al., "Surface Superconductivity in Nb for Superconducting RF Cavities", TESLA report 2004-06, 2004;
- [6] B. Bonin, "Materials for Superconducting Cavities", p. 191, Proc. of the 1995 CAS on Superconductivity in Particle Accelerators, CERN-96-03, May 1996;
- [7] J. Halbritter, "On Surface Resistance of Superconductors", Zeitschrift fuer Physik 266, p. 209, 1974;
- [8] H. Padamsee, "RF Superconductivity for Accelerators", J. Wiley & Sons, 1998;
- [9] G. Ciovati, "Effect of Low Temperature Baking on Niobium Cavities", 11th SCRF WS, Sept. 2003, Luebeck;
- [10] E. Haebel - TTF Meeting – 1998;
- [11] J. Halbritter, "Material Science of Nb RF Accelerator Cavities: Where Do We Stand 2001", Proc. RFSCWS X, Japan, 2001;
- [12] J. Knobloch et al., "High-Field Q Slope in Superconducting Cavities Due to Magnetic Field Enhancement at Grain Boundaries", Proc. RFSCWS IX, U.S.A., 1999;
- [13] B. Visentin et al., "A Non-Electropolished Niobium Cavity Reached 40 MV/m at Saclay", Proc. of 2002 European Particle Accelerator Conference, Paris 2002;
- [14] A.M. Valente et al., "Study of the Surface Resistance of Superconducting Niobium Films at 1.5 GHz", CERN, internal note EST/98-02 (SM), Sept. 1998;
- [15] L. Lilje, et al., "Improved Surface Treatment of the Superconducting TESLA Cavities", Nucl. Instr. Meth., A 516 (2-3) pp 213-227, 2004;
- [16] H. Safa, "High Field Behavior of SCRF Cavities", MA008, Proc. RFSCWS X, Jp, 2001;
- [17] Appl. Phys. Letters, N. 53(14), pp 1343, 1988;
- [18] C. Antoine, A. Aspart, S. Regnault, A. Chincarini, "Surface Studies: Method of Analysis and Results", MA007, Proc. RFSCWS X, Jp, 2001;

- [19] S. Calatroni et al. "Cern Studies on Niobium Coated 1.5 GHz Copper Cavities, MA002 – Proc. RFSCWS X, Jp 2001;
- [20] S. Calatroni et al., "Diffusion of Oxygen in Niobium During Bake-Out", PR025, Proc RFSCWS X, Jp, 2001;
- [21] K. Saito / P. Kneisel, TUP031, Proc RFSCWS X, Jp, 2001;
- [22] E. Palmieri, TL004 – Proc RFSCWS X, Jp, 2001;
- [23] R. Rosenberg, Q. Ma, "Thermal and Electron Beam Irradiation Effects on the Surfaces of Niobium for RF Cavity Production", PR007, Proc RFSCWS X, Jp, 2001;
- [24] B. Visentin, "Q-Slope at High Gradients", RFSCWSXi, Ger., 2003
- [25] H. Safa et al., "Specific Resistance Measurement of a Single Grain Boundary in Pure Niobium", Proc RFSCWS IX, USA, 1999;

APPENDIX A

Iterative Calculation of the Temperature Profile Across the Cavity Wall

The temperature profile across (discretization length Δ , number of elements M) the Nb sheet between the outer surface cooled by superfluid helium to the inside surface exposed to RF fields is calculated iteratively from a start ("guess") value for the temperature at the inside surface. The temperature in segment i (counting starts at the bath side where $T_0 = T_{b0}$) is calculated with equation (A1) from the RF power calculated from the guess value for the RF surface temperature T_{guess} . The local temperature within segment i is taken into account when calculating the local thermal conductivity κ . The temperature step due to the Kapitza resistance (conductance a_{Kap}) at the Nb-He interface is also taken into account in the calculation of the first value of the temperature array.

$$i = 1 \quad T_1 = T_{b0} + \frac{P_{RF}(T_{guess}, H_{peak}, \dots)}{a_{Kap}}, \quad i > 1 \quad T_i = T_{i-1} + \frac{P_{RF}(T_{guess}, H_{peak}, \dots)\Delta}{\kappa(T_{i-1})} \quad (A1)$$

The temperature at the RF surface is the last value in the T_i array, T_N . This temperature becomes the new guess (start) temperature for a subsequent iteration until expression (A2) is smaller than some upper threshold. When $T_N = T_{guess}$, a self-consistent set of temperatures is found and the RF heat flux generated on the inside surface becomes equal to the heat flux across the Nb wall.

$$\varepsilon = \left| \frac{\kappa \left(\frac{T_{guess} - T_{b0}}{2} \right) w}{1m^2} (T_{guess} - T_{b0} - \Delta T_{Kap}) - P_{RF}(T_{guess}) \right| \quad \left(\frac{W}{m^2} \right) \quad (A2)$$

The following plot shows typical temperature profiles across a 3 mm sheet for $P_{RF} = 80$ & 175 W/m^2 .

Not yet implemented in this model is the transition to film-boiling at ~ 10 kW/m^2 heat flux into the coolant. Also not included is 2D conduction.

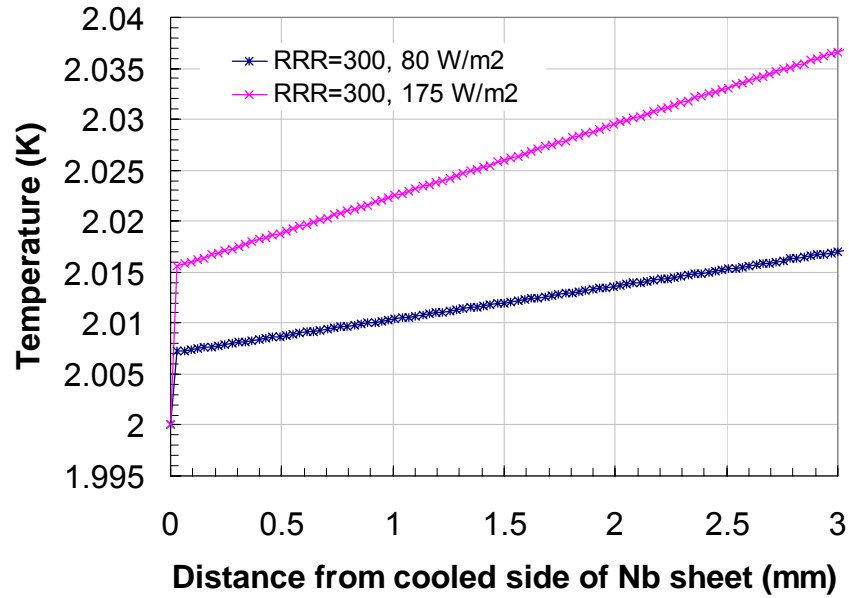


Fig. A1: Calculated temperature profile across 3 mm cavity wall for TESLA cavity (bulk Nb, RRR=300) at 2 different RF heat loads. The temperature profile was calculated with the iterative model presented above (A1-A2). Thermal conductivity of Nb as described in appendix B.

APPENDIX B**Thermal Conductivity of Niobium**

The following formalism for the thermal conductivity of high purity Niobium is from Koechlin-Bonin^[2]. Their model uses modified constants (indicated with ') and parameters to calibrate the theoretical model to measurement data. The total thermal conductivity is a sum of the electron and phonon contributions.

The electron contribution is regulated by the number of electrons at the Fermi-level, which are not condensed into the superconducting phase. A polynomial fit of the normalized superconducting electron function is (B1):

$$R(y) = 10^{-4} y^4 - 5.4 \cdot 10^{-3} y^3 + 0.1017 y^2 - 0.7848 y + 2.1282 \quad \alpha' < y < 8 \quad R(y > 8) = 1 \quad (\text{B1})$$

The electronic contributions to the thermal conductivity are given with Wiedemann-Franz ($L' = 2.11 \times 10^{-8} \text{ W}\Omega/\text{K}^2$) and electron-phonon exchange ($F_{el-phon} = 7.6 \times 10^{-7} \text{ m/W/K}$). Note that the argument of the superconducting electron function is $\alpha' T_c/T$, with $\alpha' = 1.53$, the modified BCS gap parameter.

$$\kappa_{el}(T, RRR) = R\left(\alpha' \frac{T_c}{T}\right) \frac{1}{\left(\frac{\rho(295\text{K})}{L' RRR T}\right) + F_{el-phon} T^2} \left(\frac{W}{K-m}\right) \quad (\text{B2})$$

The phonon contribution is given with $C_1 = 234 \text{ mK}^3/\text{W}$ and $C_2 = 4.34 \times 10^3 \text{ W/K}^4/\text{m}^2$; Since the material considered is of very high purity, the phonon mean free path is assumed to be the grain-size.

$$\kappa_{phon}(T) = \frac{(1 + f_{peak})}{C_1 T^{-2} e^{-\alpha' \frac{T_c}{T}} + \frac{1}{C_2 l_{mfp,phon} T^3}} \left(\frac{W}{K-m}\right) \quad (\text{B3})$$

The phonon-peak was (arbitrarily) represented by a sin-function parameterized such as to generate a peak at 2 K with an (arbitrary) amplitude $A = 20$ (B4).

$$f_{peak} = A \cdot \sin\left((T - 0.5K)\frac{\pi}{2}\right) \quad 1K < T < 3K \quad (B4)$$

A phenomenological fit for the Kapitza conductance for $T - T_b < 1.4$ K was proposed by Mittag [Cryogenics, Vol. 13, p. 94, 1973].

$$a_{Kap}(T) = 200 \cdot (T_b^{4.65}) \left[1 + 1.5 \left(\frac{T - T_b}{T_b} \right) + \left(\frac{T - T_b}{T_b} \right)^2 + 0.25 \left(\frac{T - T_b}{T_b} \right)^3 \right] \left(\frac{W}{Km^2} \right) \quad (B5a)$$

Although, not used here, a possible, simpler alternative would be:

$$a_{Kap}(T) = 200 \cdot e^{2T} \left(\frac{W}{Km^2} \right) \quad (B5b)$$

For the calculation of the Kapitza conductance (and only there) an assumption was made for the temperature on the Nb side of the interface (e.g. $T \sim T_b + 0.01$ K).

The following figure shows the Nb thermal conductivity calculated for RRR=300 and 600 with and without phonon-peak (PP).

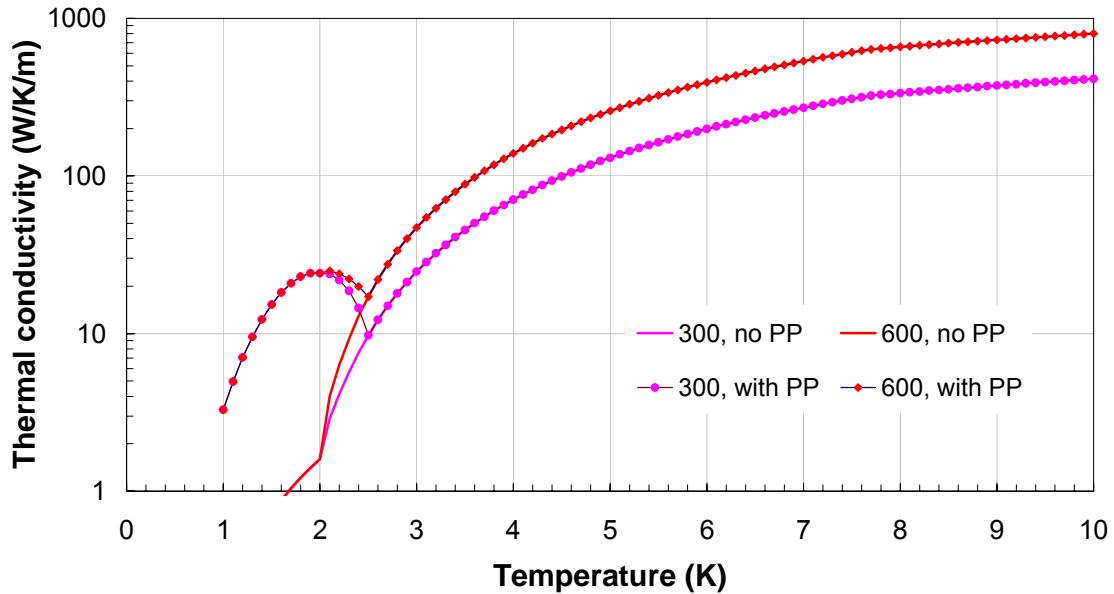


Fig. B1: Thermal conductivity of high purity Nb according to Koechlin-Bonin^[2].

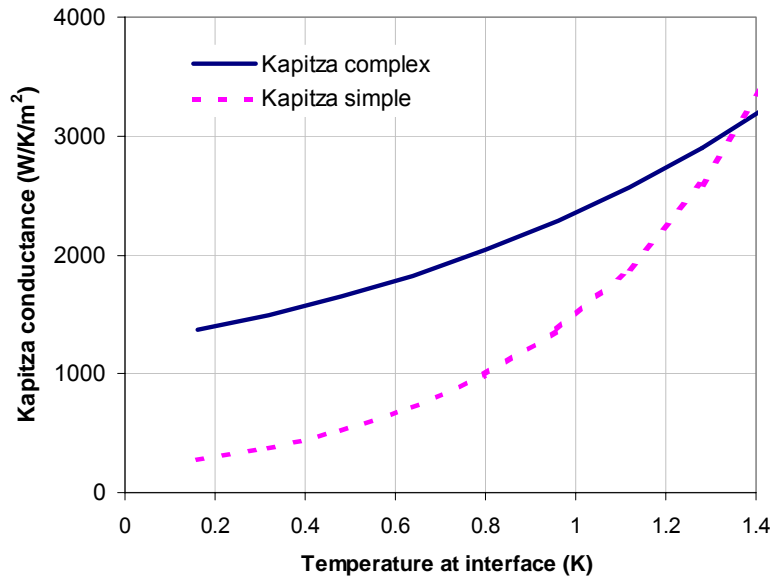


Fig. B2: Thermal Kapitza interface conductance according to the models presented in equation B5a & B5b.

The above implementation of the thermal conductivity is only applicable to bulk material not to thin films where grain boundary effects contribute. Also the presence of a phonon peak is a subject of discussion.

APPENDIX C**Normal State RF Surface Resistance of Niobium**

The normal state resistivity for normal conductors can be calculated in the classical (classical penetration depth) and the anomalous (penetration depth smaller than mean free path) limit, as shown below. There is also an intermediate formula not quoted here (see [8], p. 80). In the anomalous limit the normal state surface resistance is higher than in the classical case.

$$R_{s,normal} = \frac{1}{\delta\sigma} = \begin{cases} \sqrt{\pi f \mu_0 \rho_n (RRR)} \sim 1.5 \times 10^{-3} \Omega \quad (RRR = 300) \\ \left(\frac{\mu_0 \omega}{2}\right)^{2/3} (\rho_n l_{mfp})^{1/3} \approx 2.6 \times 10^{-3} \Omega \quad (\rho_n l_{mfp} = 6.56 \cdot 10^{-16} \Omega m^2) \end{cases} \quad (C1)$$